Synthesis, structure, magnetism and specific heat of $YCrO_4$ and its zircon-to-scheelite phase transition

Y. W. Long, L. X. Yang, Y. Yu, F. Y. Li, R. C. Yu, and C. Q. Jin*

National Laboratory for Condensed Matter Physics, Institute of Physics, Chinese Academy of Sciences, Beijing 100080, People's Republic of China

(Received 23 October 2006; revised manuscript received 3 January 2007; published 2 March 2007)

The scheelite-type $YCrO_4$ with space group $I4_1/a$ was synthesized at 6.0 GPa and 450 °C from its ambient-pressure zircon-type phase in $I4_1/amd$ symmetry. Accompanying the structural phase transition from zircon to scheelite, magnetic and specific heat properties are changed drastically. In magnetism, $YCrO_4$ will transform from being ferromagnetic with Curie temperature of about 9 K for the zircon phase to being antiferromagnetic with Néel temperature of 21 K for the scheelite phase. The magnetic superexchange interactions are rather weak due to the poor *d*-band orbital overlap. Corresponding to the magnetic transition, a λ-type anomaly in specific heat is observed in the zircon- and scheelite-type $YCrO_4$, respectively. Calculations show that the magnetic entropy changes in experiment are less than those in theory in both of the phases, especially for the scheelite phase.

DOI: 10.1103/PhysRevB.75.104402 PACS number(s): 75.30.−m, 61.50.Ks, 62.50.+p, 65.40.−b

I. INTRODUCTION

$ZrSiO_4$ is the prototype of zircon structure. It is an important phase in geophysical and geochronological investigations.[1,2] Zircon-type compounds with the chemical composition RXO_4, where *R* stands for rare-earth element and *X* is phosphorus,[3–7] vanadium,[8–13] or arsenic,[14–18] have been extensively studied due to the interesting crystallographic, magnetic, and optical properties. At appropriate pressure and/or temperature conditions, the tetragonal zircon phase with space group $I4_1/amd$ (D_{4h}^{19}, No. 141, $Z=4$) usually transforms into another tetragonal scheelite phase in $I4_1/a$ symmetry (C_{4h}^{6}, No. 88, $Z=4$). Moreover, this structural phase transition is irreversible, and the scheelite phase can be quenched to ambient conditions.[19,20] Stubican and Roy have reported a series of pressure-temperature equilibria curves for a wide variety of rare-earth arsenates and vanadates in the pressure range of 1–6 GPa.[21]

Rare-earth chromates $RCrO_4$ belong to the famous family of the zircon-type compounds. However, they have been much less studied because it is not easy to prepare pure polycrystalline samples. In particular, single crystals are more difficult to obtain taking account of the thermal instability of $RCrO_4$ compounds at high temperature. They will decompose into refractory $RCrO_3$ perovskites when temperature exceeds 700 °C. Schwarz synthesized the zircon-type $RCrO_4$ compounds through standard solid-state reaction method in the 1960s,[22] but some impurities such as Cr_2O_3 existed in their samples. Due to the unique out-shell electronic configuration of the quinquevalent chromium ions in $RCrO_4$, their magnetic structures subsequently were selectively investigated by means of neutron powder diffraction.[23,24] In the recent several years, $RCrO_4$ compounds have received renewed interest. Good single-phase samples have been prepared using correlated nitrates or acetates as original materials.[25–28] In addition, magnetic properties have also been widely studied by various experimental methods.[25–32]

$YCrO_4$ crystallizes into a tetragonal zircon-type structure at ambient condictions.[27] It is built from alternating edge-sharing CrO_4 tetrahedra and YO_8 dodecahedra. As shown in Fig. 1(a), YO_8 units are connected to each other at the *a*-axis direction. Along the *c*-axis direction, they alternately link with CrO_4 tetrahedra. Moreover, there is a slight elongation for the CrO_4 tetrahedra because the lengths of O-O edges shared with YO_8 dodecahedra are shorter than those of the unshared ones, although the Cr-O bond lengths are equal in CrO_4 units. Unlike other zircon-type compounds mentioned above, little is still known on the high-pressure structural and physical properties of $RCrO_4$. We have recently observed a pressure-induced irreversible crystal structural phase transition from zircon to scheelite in $YCrO_4$ by using high-pressure Raman scattering techniques at room temperature.[33] Moreover, the phase transition is sluggish under high hydrostatic pressure. It occurs at 3.0 GPa, but is not completed until 15.1 GPa. Since both temperature and pressure are jointly important parameters that influence the material's thermodynamic state, it is possible to synthesize a bulk $YCrO_4$ with scheelite-type structure at appropriate temperature and pressure conditions. Because the scheelite phase is

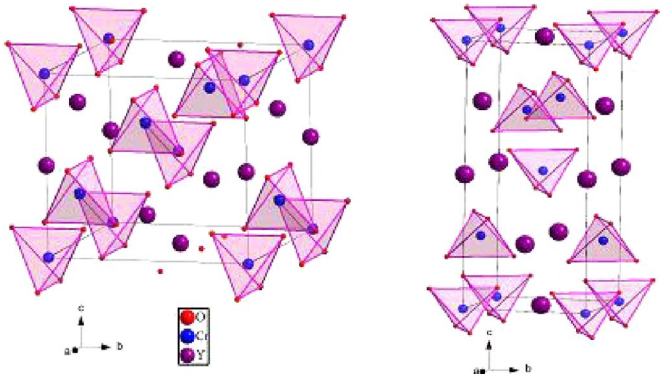

FIG. 1. (Color online) (a) The zircon-type and (b) scheelite-type crystal structures of $YCrO_4$. The large, medium, and small balls present Y, Cr, and O atoms, respectively. To better illustrate the relative arrangement of cations, the origins of the unit cells are chosen at Cr positions.

quenchable, it will enable us to study the structural and physical properties in detail at ambient pressure.

In this paper, we report the high-pressure synthesis of the scheelite-type $YCrO_4$ from the ambient-pressure zircon phase. In addition, the crystal structure, magnetic and specific heat properties are comparatively studied on the ambient-pressure zircon phase and the high-pressure scheelite phase.

II. EXPERIMENT

A. Sample preparation

The polycrystalline powder sample of the zircon-type $YCrO_4$ was prepared by using stoichiometric $Y(NO_3)_3 \cdot 6H_2O$ and $Cr(NO_3)_3 \cdot 9H_2O$ with analytical purity as starting materials.[32] After complete mixing, the mixture was heated according to the following heat treatment in air: 2 °C/min to 160 °C for 30 min, 2 °C/min to 200 °C for 30 min, and 10 °C/min to 580 °C for 60 min. In order to improve the crystallography, it is useful for the green product to be annealed in oxygen at 280 °C for 6 h. Powder x-ray diffraction (XRD) pattern confirmed that the final product has a pure zircon-type phase.

Scheelite-type $YCrO_4$ was synthesized from the zircon-type powder sample. It was pressed into a pellet with 6 mm in diameter and 2 mm in height. The pellet was inserted into a pyrophyllite assembly after being packaged in a Au foil. Graphite tube was used as a heater. Pressure was generated by a set of cubic anvil apparatus, where the maximum pressure and temperature can reach 6.0 GPa and 1600 °C, respectively. When pressure gradually increased to 6.0 GPa with a rate of 2 GPa/min, the sample was heated to 400 °C (150 °C/min) for 10 min. After reaction, the sample was quenched to room temperature and then the pressure was gradually released. A black product with a tetragonal scheelite-type structure was obtained.

B. Structural analysis

X-ray powder diffraction experiments were performed on both the zircon and scheelite compounds by using a Rigaku diffractometer equipped with a monochromator (Cu Kα radiation, 50 kV, 200 mA). Diffraction data were collected in the angle (2θ) range from 15° to 125° with a step of 0.02°. The counting time is 5 s for each step. Crystallographic parameters were analyzed by Rietveld full-profile refinement using the GSAS program.[34]

C. Magnetic and specific heat measurements

The temperature (T) and field dependence of the magnetization (M) were measured by using a commercial superconducting quantum interference device magnetometer (MPMS-5, Quantum Design) after zero-field cooling. For the susceptibility-temperature curves, measurements were performed on heating in a fixed field (100 Oe). At several selected temperatures, the magnetization curves were measured in the applied field from −3 to 3 T. Specific heat measurements were done using a Quantum Design PPMS calorimeter. The data were collected on cooling from 100 to 2 K.

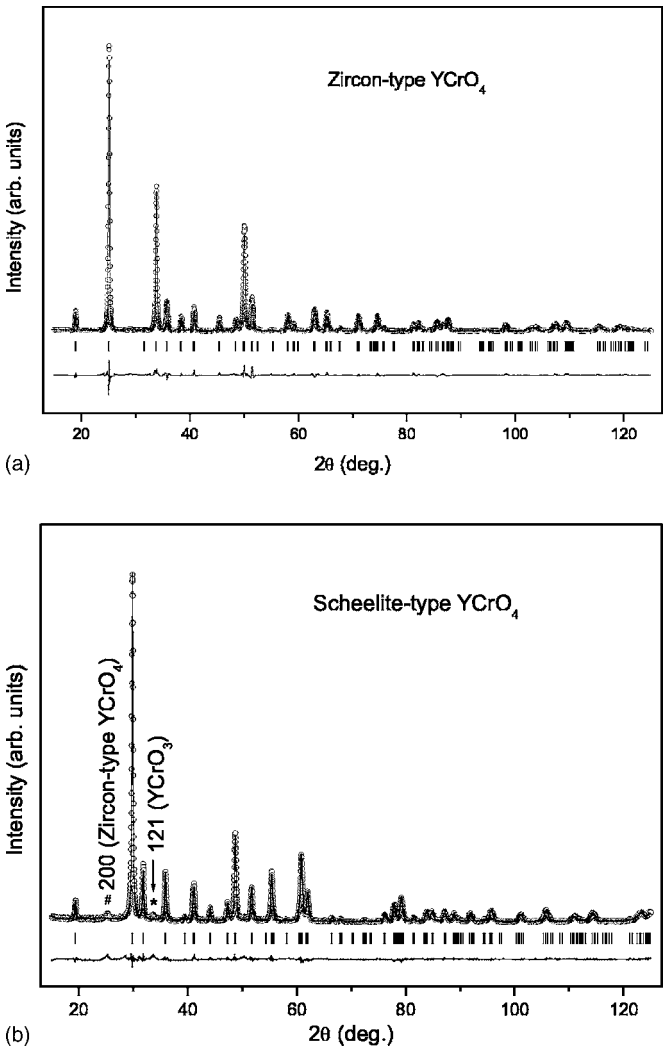

FIG. 2. Observed (o), calculated (solid line), and difference (below) XRD patterns for (a) the zircon-type and (b) scheelite-type $YCrO_4$. Tick marks show the allowed Bragg reflections. The diffraction peaks marked with "*" and "#" in (b) result from the reflection of $YCrO_3$ and the residual zircon phase, respectively.

III. RESULTS AND DISCUSSION

A. Crystal structures

Figures 2(a) and 2(b) show the results of Rietveld analysis on the powder XRD patterns of the zircon- and scheelite-type $YCrO_4$, respectively. The observed, calculated, and difference patterns as well as the allowed reflection peaks are exhibited in the figures. For the zircon phase, all the Bragg reflections can be indexed based on the $I4_1/amd$ space group with the reflection conditions $h+k+l=2n$; $l=0$, h, $(k)=2n$; $h=0$, $k+l=2n$; and $h=k$, $2h+l=4n$. Y, Cr, and O atoms occupy the special sites 4a (0, 3/4, 1/8), 4b (0, 1/4, 3/8), and 16 h (0, y, z), respectively. The crystallographic data such as lattice parameters, atomic positions of oxygen, bond lengths, and angles are presented in Tables I and II.

TABLE I. Crystallographic data for the zircon- and scheelite-type $YCrO_4$.

	Zircon type	Scheelite type
Space group	$I4_1/amd$	$I4_1/a$
a (Å)	7.1074(3)	5.0030(2)
c (Å)	6.2486(3)	11.2636(4)
c/a	0.879	2.251
V (Å^3)	315.65(4)	281.93(3)
Z	4	4
D_{cal} (g cm^{-3})	4.311	4.827
O_x	0	0.2559(9)
O_y	0.4351(4)	0.1035(7)
O_z	0.2028(4)	0.0480(3)
B_Y (Å^2)	0.006	0.001
B_{Cr} (Å^2)	0.007	0.004
B_O (Å^2)	0.022	0.017
R_{wp} (%)	9.17	6.56
R_p (%)	7.41	5.10

As far as the scheelite phase is concerned, its Bragg reflections can be indexed according to the $I4_1/a$ symmetry with the reflection conditions $h+k+l=2n$; $l=0$, h, $(k)=2n$; and $h=k=0$, $l=4n$. In this symmetry, Y and Cr atoms occupy the special positions $4b$ (0, 1/4, 5/8) and $4a$ (0, 1/4, 1/8), respectively, and oxygen atom occupies a general site as given in Table I. The corresponding structural parameters for the scheelite phase are also listed in Tables I and II.

Note that a few of $YCrO_3$ impurities (5.6% in volume percent according to the refinement results) are observed as represented by the diffraction peak marked with an asterisk in Fig. 2(b) due to the thermal sensitivity of chromium(v) ions in $YCrO_4$. In addition, the peak noted with a "#" sign results from the diffraction of the residual zircon phase. However, these few impurities will not influence the inherent physical properties of the scheelite phase as will be discussed later. Based on the high-pressure Raman scattering experiment,[33] 15.1 GPa is needed to complete the zircon-scheelite structural transition in $YCrO_4$ at room temperature. However, the available pressure is 6.0 GPa in our high-pressure synthesis apparatus. We regard that the impurity phases mentioned above would be excluded if the synthesis pressure was increased and the reaction temperature was decreased simultaneously. The optimized synthesis conditions we infer are 8–10 GPa and 350–400 °C.

TABLE II. Selected bond lengths (Å) and angles (deg) in CrO_4 and YO_8 polyhedra in the zircon- and scheelite-type $YCrO_4$.

	Zircon type	Scheelite type
	CrO_4	
Cr-O	1.700(3) (4×)	1.711(4) (4×)
O-Cr-O	101.43(17) (2×)	119.12(24) (2×)
	113.63(9) (4×)	104.87(11) (4×)
	YO_8	
Y-O	2.290(3) (4×)	2.318(4) (4×)
	2.434(3) (4×)	2.414(4) (4×)

According to the crystallographic data, the crystal structure of the scheelite-type $YCrO_4$ is plotted as shown in Fig. 1(b). Just like the zircon phase, each Y/Cr ion is also coordinated by eight/four O ions forming YO_8/CrO_4 dodecahedral/tetrahedral units in the scheelite phase. In addition, all the CrO_4 tetrahedral units are relatively isolated. From Table I it is known that the theoretical density and the lattice-axis ratio of c/a in the scheelite phase will increase by about 10.7% and 156%, respectively, when compared with those of the zircon phase.

In an earlier study on $ZrSiO_4$ using shock loading method, Kusaba *et al.*[35] have proposed a two-step mechanism for the structural phase transition from zircon to scheelite, where only simple shearing and small displacements of atoms were involved. According to their description, the density will increases by about 10% in this structural transition, which agrees well with our experimental result. In addition, they claimed that no bond breaking as well as no long-range diffusion of atoms occurred in the zircon-scheelite transition, only that a more efficient packing in the scheelite phase is obtained mostly by cooperative rotation of SiO_4 units. Unlike the fast conversion of $ZrSiO_4$ under shock compression, the structural transition of $YCrO_4$ is sluggish under hydrostatic pressure and room temperature as shown by our high-pressure Raman scattering.[33] It suggests that partially long-range diffusion of atoms may be involved in hydrostatic pressure condition. Furthermore, structural refinements show that there are remarkable changes in Cr-O-Cr bond angles in CrO_4 units between the zircon and scheelite phases (see Table II). In our view, therefore, the zircon-scheelite transition should involve a more drastic change, including polyhedral distortions and rotations. These results cause a more efficient packing of the coordination polyhedra as well as the elimination of structural voids in the zircon phase. All of these are responsible for the large increase in density in the zircon-scheelite transition. The abrupt changes in Raman spectra also gave convincing evidence for this drastic structural conversion.[33] Similar results were also reported by Jayaraman and co-workers in RVO_4 (R=Y, Tb, Dy).[9,10]

B. Magnetic properties

Figure 3 shows the temperature dependence of the inverse susceptibility (χ^{-1}) of the zircon-type $YCrO_4$. A ferromagnetic transition is observed at about 9 K as displayed evidently in the inset, which represents the χ-T relationship in 5–20 K. The susceptibility data above 20 K can be fitted well using the Curie-Weiss law with the expression $\chi^{-1}=(T-\theta)/C$, where θ denotes the Weiss constant and C is the Curie constant. The solid line in Fig. 3 shows the fitting result. The constants θ and C are fitted to be 6.8±0.4 K and 0.409±0.001 Kemu/mol, respectively. According to the formula $\mu_{eff}=\sqrt{3k_Bc/N_A}$ (k_B and N_A are the Boltzmann constant and the Avogadro number, respectively), the effective magnetic moment μ_{eff} is determined to be $1.81\mu_B$, which is quite close to the theoretical value ($2\sqrt{s(s+1)}\mu_B=1.73\mu_B$) on a Cr^{5+} ion with spin $s=1/2$ in $YCrO_4$.

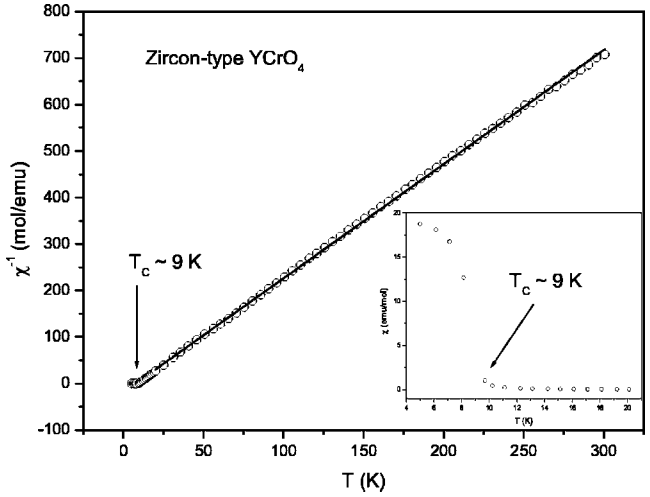

FIG. 3. Temperature dependence of the inverse susceptibility of the zircon-type $YCrO_4$. The solid line shows the Curie-Weiss fitting result. Inset shows the relationship of susceptibility vs temperature in 5–20 K.

The positive Weiss constant is indicative of ferromagnetic interactions in the zircon-type $YCrO_4$. In order to testify the existence of ferromagnetic component, magnetization measurements were performed at 5 and 20 K, respectively, as shown in Fig. 4. The magnetization increases sharply with the applied field and tends to saturate only when the field reaches 0.3 T at 5 K. In addition, it is almost independent of the history of the applied field. This means that the sample is a soft magnet below the Curie temperature. Based on the experimental data, the saturated moment is determined to be $0.80\mu_B$ at 5 K, somewhat less than the completely saturated value of a Cr^{5+} ion ($1\mu_B$). When temperature is set to 20 K, the *M*-*H* curve exhibits a good linear relationship. It is consistent with the paramagnetic characteristic, as presented by the susceptibility measurement.

For the scheelite-type $YCrO_4$, the temperature dependence of the inverse susceptibility is shown in Fig. 5. Be-

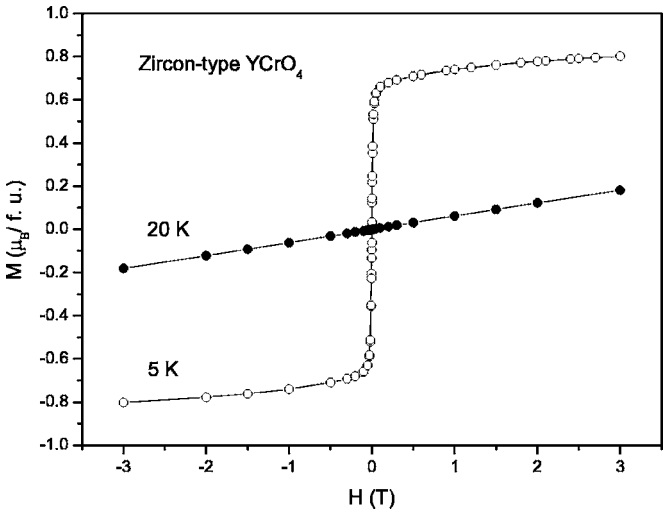

FIG. 4. Magnetization curves of the zircon-type $YCrO_4$ at 5 and 20 K.

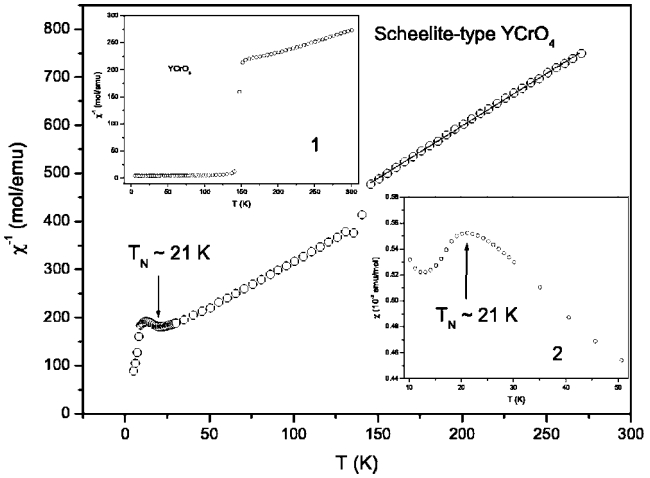

FIG. 5. Temperature dependence of the inverse susceptibility of the scheelite-type $YCrO_4$. The solid line shows the Curie-Weiss fitting result. Inset 1 shows the relationship of inverses susceptibility vs temperature for $YCrO_3$. Inset 2 shows the relationship of susceptibility vs temperature in 10–50 K for the scheelite-type $YCrO_4$.

cause there exists a few $YCrO_3$ impurities, which exhibit a sharp weak ferromagnetic transition at 146 K (Ref. 36) as presented in inset 1, a small jump is observed at the same temperature in the scheelite phase of $YCrO_4$, but it is interesting that an antiferromagnetic transition appears around 21 K. Inset 2, which presents the χ-T relationship in 10–50 K, shows the transition more clearly. The inverse susceptibility varies linearly with temperature in 150–270 K. Based on the Curie-Weiss fitting, the Weiss constant and the effective moment are determined to be -75.5 ± 1.3 K and $1.92\mu_B$, respectively. The negative Weiss constant is a hint of antiferromagnetic interactions. The calculated effective moment in the scheelite phase is slightly larger than that of the zircon phase ($1.81\mu_B$), which we think is related to the presence of a small amount of Cr^{3+} ions arisen from $YCrO_3$ impurities in the scheelite phase.

In order to explore the influence of the ferromagnetic impurities (including the zircon-type $YCrO_4$ and $YCrO_3$) on the magnetism of the scheelite-type $YCrO_4$ at low temperature, magnetization measurements were made at 5 and 20 K, respectively, as shown in Fig. 6. Unlike the sharp increase of magnetization in the zircon-type $YCrO_4$ at lower field, the magnetization almost linearly changes with field in the scheelite-type $YCrO_4$. In the weak ferromagnetic $YCrO_3$ perovskite, hysteresis loops have been observed clearly below T_C, and the coercive field reaches 1.6 T at 5 K.[36] However, no visible hysteresis loop is explored in the scheelite-type $YCrO_4$. We therefore believe that the antiferromagnetic transition observed at 21 K is an inherent characteristic feature of the scheelite-type $YCrO_4$, and the influence of the ferromagnetic impurities on the magnetism is not important below T_N.

As is shown by the structural analysis, the CrO_4 tetrahedra are isolated from one another both in the zircon- and scheelite-type $YCrO_4$. Thereby two oxygen atoms are involved in the ferromagnetic as well as in the antiferromag-

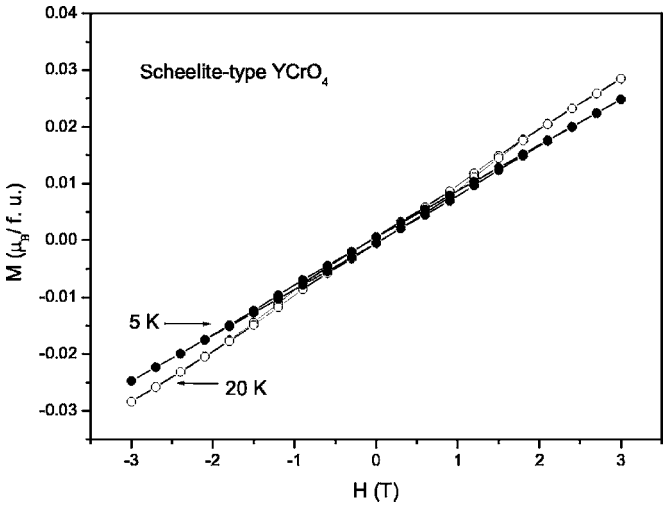

FIG. 6. Magnetization curves of the scheelite-type $YCrO_4$ at 5 and 20 K.

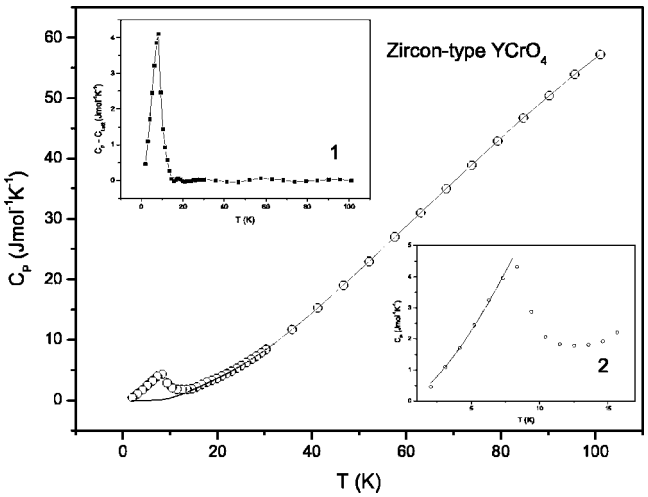

FIG. 7. Temperature dependence of specific heat for the zircon-type $YCrO_4$. The solid line shows the fitting result using the Einstein model. Inset 1 presents the ferromagnetic transition contribution to specific heat. Inset 2 presents the fitting result based on the Debye model associated with the ferromagnetic excitation in 2–8 K.

netic superexchange interactions with the sequence Cr^{5+}-O-O-Cr^{5+} in $YCrO_4$, where a considerably large Cr^{5+}-Cr^{5+} distance occurs. For example, the nearest neighbor Cr^{5+}-Cr^{5+} distances are 3.88 and 3.77 Å in the *ac* plane for the zircon and scheelite phases at room temperature, respectively. The exchange integral sign will be changed due to the varieties of the nearest neighbor Cr^{5+}-Cr^{5+} distances during the structural phase transition. Therefore, different magnetic properties are exhibited in the zircon- and scheelite-type $YCrO_4$. Actually, the superexchange interactions in $YCrO_4$ are rather weak on account of the poor *d*-band orbital overlap of Cr^{5+} ions. It probably is expectable that the magnetic transition temperature or even the magnetic structure of $YCrO_4$ can be effectively tuned by using appropriate external conditions such as high pressure and/or strong field. It is therefore interesting to investigate the magnetic properties of $YCrO_4$ under high hydrostatic pressure.

C. Specific heat properties

Figure 7 shows the temperature dependence of specific heat (C_P) of the zircon-type $YCrO_4$. Because there exists a magnetic structural transition, a λ-type anomaly in C_P is also observed at about 9 K. The zircon-type $YCrO_4$ is an electric insulator, thereby the C_P can be attributed to the contribution of phonon (C_{ph}). Above 20 K, C_P can be fitted well using the Einstein model, as shown by the solid line presented in Fig. 7. When extrapolated to room temperature, C_P value increases to 104.1 J mol^{-1} K^{-1}, agreeing with the Dulong-Petit law, which gives the critical value of molar specific heat to be 3*NR* for an ideal system at high-temperature limit, where *N* is the number of atoms in each molecule and *R* is the gas constant. In order to calculate the magnetic entropy change ΔS, we extrapolate the Einstein fitting curve to 2 K as the phonon background, then ferromagnetic excitation contribution to C_P is determined by subtracting the phonon background from the total C_P. Inset 1 of Fig. 7 shows the subtracted result. Finally, according to the integral formula $\Delta S = \int_{T_i}^{T_f}(C_P - C_{ph})/TdT$, where T_i and T_f are two temperatures conveniently chosen to present the interval of interest, ΔS is determined to be 4.2 ± 0.6 J mol^{-1} K^{-1}. In theory, the entropy change for the independent spin order in $YCrO_4$ should be $\Delta S_{th} = \Delta S_{Cr^{5+}} = R \ln(2S+1) = 5.76$ J mol^{-1} K^{-1}. The "missing" entropy between the experimental and theoretical values partially results from the imprecise subtraction of phonon background, but mostly we think it results from an incomplete ferromagnetic order at T_C in the zircon-type $YCrO_4$, as described in Ref. 37. In fact, the lower saturated moment of Cr^{5+} ion shown in Fig. 4 implies the incomplete ferromagnetic polarization.

Below the anomalous transition temperature (2–8 K), C_P can be finely fitted based on the Debye model associated with the ferromagnetic excitation contribution using the function $C_P = \alpha T^3 + \beta T^{3/2}$,[38] where α and β present the phonon and ferromagnetic contributions to C_P, respectively. The solid line in inset 2 of Fig. 7 shows the fitting result, and the coefficients α and β are simulated to be 0.0004 J mol^{-1} K^{-4} and 0.202 J mol^{-1} $K^{-5/2}$, respectively. Evidently, ferromagnetic contribution to the total C_P is much larger than that of the phonon in the zircon-type $YCrO_4$ at low temperature. According to the coefficient α, the Debye temperature Θ_D was calculated to be 308 K using the formula $\Theta_D = (12\pi^4 NR/5\alpha)^{1/3}$. It is a typical value reported on most oxides.[37]

As the scheelite-type $YCrO_4$ is considered, the C_P-*T* curve is shown in Fig. 8. Corresponding to the antiferromagnetic transition that happens at 21 K, a λ-type anomaly in specific heat is also found at the same temperature. The specific heat data above 30 K can be fitted well using the Einstein model, as shown by the solid line in Fig. 8. Theoretical extrapolation of C_P to room temperature is 100.5 J mol^{-1} K^{-1}, slightly less than that of the zircon phase mentioned above (104.1 J mol^{-1} K^{-1}). Based on the Dulong-Petit law, it seems to imply a little decomposition of $YCrO_4$ into $YCrO_3$ as we observed in the XRD pattern. The

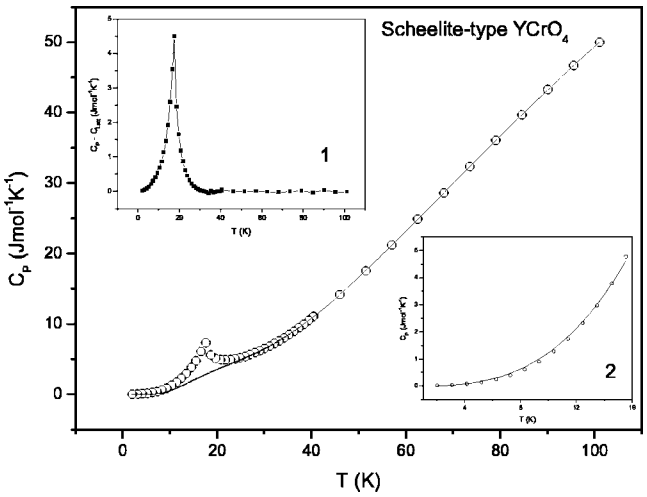

FIG. 8. Temperature dependence of specific heat for the scheelite-type $YCrO_4$. The solid line shows the fitting result using the Einstein model. Inset 1 presents the antiferromagnetic transition contribution to specific heat. Inset 2 presents the fitting result based on the Debye model associated with the antiferromagnetic excitation in 2–18 K.

scheelite-type $YCrO_4$ also exhibits electrical insulating behavior, where the C_P is ascribed to the phonon contribution in 30–100 K. Using the same method described in the zircon-type phase, the ΔS of the scheelite phase is determined to be 1.8 ± 0.2 J mol^{-1} K^{-1}. This value is much less than what one would expect from a complete spin order (ΔS_{th}) on a Cr^{5+} ion. It suggests that a fully antiferromagnetic ordering state probably is only complete well below T_N in the scheelite-type $YCrO_4$. Alternatively, a considerable amount of entropy associated with the antiferromagnetic transition may be given up at the temperatures higher than T_N due to the existence of some short-range correlations, so that only a part of the magnetic contribution to specific heat is involved within the integral temperature range we used. Some analogous results were also reported in many other oxides.[37,39,40]

Between the temperature range from 2 to 18 K, the C_P of the scheelite phase can be fitted well using a simple function $C_P = \gamma T^3$, as shown by inset 2 in Fig. 8. The coefficient γ is determined to be $0.001\,29 \pm 0.000\,02$ J mol^{-1} K^{-4}. Because both phonon and antiferromagnetic excitation contributions to C_P are proportional to T^3 at low temperature, one cannot accurately determine which part is the dominant component. However, by comparison with the case of the zircon phase, we infer that the antiferromagnetic contribution to C_P may be more important than that of the phonon at lower temperature in the scheelite-type $YCrO_4$.

IV. CONCLUSION

In summary, we prepared the scheelite-type $YCrO_4$ from the zircon phase at 6.0 GPa and 450 °C. Some drastic changes in bond angles, theoretical density, and lattice-axis ratio of c/a happened in the zircon-scheelite structural transition although the coordination numbers of the cations (Y/Cr) are invariable. The zircon phase exhibits a soft magnetic behavior, and a ferromagnetic transition is observed around 9 K. Specific heat anomaly also occurs at the same temperature. The specific heat is mainly ascribed to the ferromagnetic contribution below the Curie temperature. The scheelite-type $YCrO_4$ experiences an antiferromagnetic transition at 21 K, where a λ-type anomaly in specific heat is observed. By using the integral formula $\Delta S = \int_{T_i}^{T_f} (C_P - C_{ph})/TdT$, we calculated the magnetic entropy changes in both the zircon and scheelite phases. A notable "missing" entropy change between the experimental and theoretical values is found in the scheelite phase. It points out an incomplete spin order at T_N in this phase.

ACKNOWLEDGMENTS

This work was partly supported by the National Natural Science Foundation and the Ministry of Science & Technology of China through the research projects.

*Electronic address: jin@aphy.iphy.ac.cn

[1] A. P. Dickin, *Radiogenic Isotope Geology*, (Cambridge University Press, New York, 1995), p. 490.
[2] *Reviews in Mineralogy*, edited by J. M. Hanchar and P. W. O. Hoskin, (Mineralogical Society of America, Washington, D.C. 2003), Vol. 53.
[3] J. Sivardiere, Phys. Rev. B **8**, 2004 (1973).
[4] H. Meyssamy, K. Riwotzki, A. Kornowski, S. Naused, and M. Haase, Adv. Mater. (Weinheim, Ger.) **11**, 840 (1999).
[5] K. Riwotzki, H. Meyssamy, H. Schnablegger, A. Kornowski, and M. Haase, Angew. Chem., Int. Ed. **40**, 573 (2001).
[6] S. Nishihama, T. Hirai, and I. J. Komasawa, J. Mater. Chem. **12**, 1053 (2002).
[7] W. H. Di, X. J. Wang, B. J. Chen, and X. X. Zhao, Chem. Lett. **34**, 566 (2005).
[8] A. H. Cooke, D. M. Martin, and M. R. Wells, Solid State Commun. **9**, 519 (1971).
[9] A. Jayaraman, G. A. Kourouklis, G. P. Espinosa, A. S. Cooper, and L. G. Van Uitert, J. Phys. Chem. Solids **48**, 755 (1987).
[10] S. J. Duclos, A. Jayaraman, G. A. Kourouklis, A. S. Cooper, and R. G. Maines, J. Phys. Chem. Solids **50**, 769 (1989).
[11] X. Wang, I. Loa, K. Syassen, M. Hanfland, and B. Ferrand, Phys. Rev. B **70**, 064109 (2004).
[12] C. J. Jia, L. D. Sun, F. Luo, X. C. Jiang, L. H. Wei, and C. H. Yan, Appl. Phys. Lett. **84**, 5305 (2004).
[13] J. K. Jabczynski, W. Zendzian, and J. Kwiatkowski, Opt. Express **14**, 2184 (2006).
[14] J. C. Wright and H. W. Moos, Phys. Rev. B **4**, 163 (1971).
[15] B. Pilawa, J. Phys.: Condens. Matter **3**, 655 (1991).
[16] O. Guillot-Noel, D. Simons, and D. Gourier, J. Phys. Chem. Solids **60**, 555 (1999).
[17] U. Kolitsch and D. Holtstam, Eur. J. Mineral. **16**, 117 (2004).

[18] M. Schmidt, A. Muller, R. C. Gil, E. Milke, and M. Binnewies, Z. Anorg. Allg. Chem. **631**, 1154 (2005).
[19] Y. W. Long, W. W. Zhang, L. X. Yang, Y. Yu, R. C. Yu, S. Ding, Y. L. Liu, and C. Q. Jin, Appl. Phys. Lett. **87**, 181901 (2005).
[20] Y. W. Long, L. X. Yang, S. J. You, Y. Yu, R. C. Yu, C. Q. Jin, and J. Liu, J. Phys.: Condens. Matter **18**, 2421 (2006).
[21] V. S. Stubican and R. Roy, J. Appl. Phys. **34**, 1888 (1963).
[22] H. Schwarz, Z. Anorg. Allg. Chem. **322**, 1 (1963); **322**, 15 (1963); **322**, 129 (1963); **322**, 137 (1963).
[23] G. Buisson, F. Tcheou, F. Sayetat, and K. Scheunemann, Solid State Commun. **18**, 871 (1976).
[24] M. Steiner, H. Dachs, and H. Ott, Solid State Commun. **29**, 231 (1979).
[25] E. Jimenez, J. Isasi, and R. S. Puche, J. Alloys Compd. **312**, 53 (2000).
[26] R. S. Puche, E. Jimenez, J. Isasi, M. T. F. Diaz, and J. L. G. Munoz, J. Solid State Chem. **171**, 161 (2003).
[27] T. Keitaro, D. Yoshihiro, and H. Yukio, J. Mater. Chem. **12**, 1189 (2002).
[28] K. Tezuka and Y. Hinatsu, J. Solid State Chem. **160**, 326 (2001).
[29] E. Jimenez, J. Isasi, and R. S. Puche, J. Solid State Chem. **164**, 313 (2002).
[30] E. Jimenez, J. Isasi, M. T. Fernandez, and R. S. Puche, J. Alloys Compd. **344**, 369 (2002).
[31] E. Jimenez, P. Bonville, J. A. Hodges, P. C. M. Gubbens, J. Isasi, and R. S. Puche, J. Magn. Magn. Mater. **272**, 571 (2004).
[32] E. J. Melero, N. H. Van Dijk, W. H. Kraan, P. C. M. Gubbens, J. Isasi, and R. S. Puche, J. Magn. Magn. Mater. **288**, 1 (2005).
[33] Y. W. Long, L. X. Yang, Y. Yu, F. Y. Li, R. C. Yu, S. Ding, Y. L. Liu, and C. Q. Jin, Phys. Rev. B **74**, 054110 (2006).
[34] A. C. Larson and R. B. Von Dreele, Los Alamos National Laboratory Report No. LAUR 86–748, 2004 (unpublished).
[35] K. Kusaba, T. Yagi, M. Kikuchi, and Y. Syono, J. Phys. Chem. Solids **47**, 675 (1986).
[36] C. R. Serrao, A. K. Kundu, S. B. Krupanidhi, U. V. Waghmare, and C. N. R. Rao, Phys. Rev. B **72**, 220101(R) (2005).
[37] M. R. Lees, O. A. Petrenko, G. Balakrishnan, and D. M. Paul, Phys. Rev. B **59**, 1298 (1999).
[38] E. S. R. Gopal, *Specific Heats at Low Temperatures* (Plenum, New York, 1966).
[39] A. K. Raychaudhuri, A. Guha, I. Das, R. Rawat, and C. N. R. Rao, Phys. Rev. B **64**, 165111 (2001).
[40] J. Lopeza and O. F. De Lima, J. Appl. Phys. **94**, 4395 (2003).